Neurobiology of Aging 82 (2019) 88–101

Contents lists available at ScienceDirect

Neurobiology of Aging

journal homepage: www.elsevier.com/locate/neuaging

The neuritic plaque in Alzheimer's disease: perivascular degeneration of neuronal processes

Gurpreet Kaur Hansra [a], Glib Popov [a], Patricia O. Banaczek [a], Monica Vogiatzis [a], Thuvarahan Jegathees [a], Claire S. Goldbury [a,b], Karen M. Cullen [a,*]

[a] Discipline of Anatomy & Histology, School of Medical Sciences, Faculty of Medicine and Health, University of Sydney, New South Wales, Australia
[b] Brain and Mind Centre, Faculty of Medicine and Health, University of Sydney, New South Wales, Australia

ARTICLE INFO

Article history:
Received 14 March 2018
Received in revised form 27 June 2019
Accepted 28 June 2019
Available online 4 July 2019

Keywords:
Alzheimer's disease
Cerebrovasculature
Dystrophic neurites
Microhemorrhage
Neuritic plaque
tau

ABSTRACT

Cerebrovascular pathology is common in aging and Alzheimer's disease (AD). The microvasculature is particularly vulnerable, with capillary-level microhemorrhages coinciding with amyloid beta deposits in senile plaques. In the current analysis, we assessed the relationship between cerebral microvessels and the neuritic component of the plaque in cortical and hippocampal 50- to 200-μm sections from 11 AD, 3 Down syndrome, and 7 nondemented cases in neuritic disease stages 0–VI. We report that 77%–97% of neuritic plaques are perivascular, independently of disease stage or dementia diagnosis. Within neuritic plaques, dystrophic hyperphosphorylated tau–positive neurites appear as clusters of punctate, bulbous, and thread-like structures focused around capillaries and colocalize with iron deposits characteristic of microhemorrhage. Microvessels within the neuritic plaque are narrowed by 1.0 ± 1.0 μm–4.4 ± 2.0 μm, a difference of 16%–65% compared to blood vessel segments with diameters 7.9 ± 2.0–6.4 ± 0.8 μm ($p < 0.01$) outside the plaque domain. The reduced capacity of microvessels within plaques, frequently below patency, likely compromises normal microlocal cerebrovascular perfusion. These data link the neuritic and amyloid beta components of the plaque directly to microvascular degeneration. Strategies focused on cerebrovascular antecedents to neuritic dystrophy in AD have immediate potential for prevention, detection, and therapeutic intervention.

1. Introduction

The classic neuropathology of Alzheimer's disease (AD) is defined by neurofibrillary tangles and senile plaques containing dystrophic neurites and extracellular amyloid beta (Aβ) deposits. Disruption of neural circuitry by neurofibrillary degeneration, marked by the accumulation of hyperphosphorylated tau (Hp-tau) fibrils in dystrophic neurites and tangles within neuronal somata parallels the severity and pattern of functional decline in AD (Arriagada et al., 1992; Bancher et al., 1993; Braak and Braak, 1991). Early cognitive symptoms correlate well with the distribution of neurite-containing plaques (NPs) (Tiraboschi et al., 2004). The spatial, temporal, and pathogenic interaction between tau derangement and Aβ deposition has provoked ongoing lively debate. Central to this debate are questions about which component of the classic plaque appears first: Hp-tau or Aβ, whether their formation is independent or whether these components interact to produce the AD syndrome. Alternatively, it is plausible that both Hp-tau and Aβ components result from an independent insult that precipitates the formation and progression of the senile plaque. This independent factor, we suggest, is degeneration of the microvasculature.

Evidence over several decades provides substantial evidence that the cerebral microvasculature is vulnerable in AD (Breteler et al., 1998; Cullen et al., 2006; Kalaria, 2002; Kumar-Singh et al., 2005; Rovelet-Lecrux, 2006). Cerebrovascular abnormalities in AD have been consistently observed since the earliest descriptions of the disease (Macchi et al., 1997). Large vessel pathology is present in a majority of AD cases (Jellinger, 2002; Roher et al., 2003). Microvessels show significant pathologic changes (Brown et al., 2000; Buee et al., 1994; Cullen et al., 2005; De La Torre, 2000; Grammas et al., 2002; Hunter et al., 2012; Kalaria and Hedera, 1995), and a disrupted blood-brain barrier correlates with early cognitive decline (Montagne et al., 2015; Nation et al., 2019). Hypoperfusion is consistently seen in AD from very early stages (De Jong et al., 1999; De La Torre, 2000), potentially precipitating and exacerbating Aβ deposition (Okamoto et al., 2012). There are near-term

* Corresponding author at: Discipline of Anatomy and Histology, School of Medical Sciences, Faculty of Medicine and Health, University of Sydney, New South Wales 2006, Australia. Tel.: +61 2 9351 2696; fax: +61 2 9351 2813.
E-mail address: karen.cullen@sydney.edu.au (K.M. Cullen).

0197-4580/$ – see front matter
https://doi.org/10.1016/j.neurobiolaging.2019.06.009

gains in understanding AD neurodegeneration, progression, and prevention by reconciling this nexus between large vessel and small vessel pathology.

Study of the microvasculature in AD has been overshadowed by other research pathways. The notion that AD is a capillary-based dementia (De La Torre, 2000; Farkas et al., 2000), or that cerebrovascular pathology is, at the very least, a core contributor to the dementia syndrome is supported by several evidence-based hypotheses for the origin and progression of AD (Hawkes et al., 2013; Hunter et al., 2012; Kalaria, 2002; Love and Miners, 2016; Saito and Ihara, 2016; Scheibel et al., 1989; Zlokovic, 2005). Rather than a downstream process additional to plaques and tangles, we suggest here that microvascular pathology is the initial insult in AD pathogenesis, with the classic plaque containing dystrophic neurites and Aβ forming subsequently to microvascular compromise.

The Aβ component of AD plaques has been shown to occur along the neurovascular interface and to colocalize with markers of microhemorrhage such as iron, clotting factors, endothelial debris, autofluorescence, and astrocytic scars (Cullen, 1997; Cullen et al., 2005, 2006). This association between microhemorrhages and extracellular deposits of Aβ prompted the current investigation into the relationship between the neurofibrillary component of the plaque and the microvasculature. Several reports link neuritic pathology to microvascular pathology in AD (Delacourte et al., 1987), head injury, and animal models (Li et al., 2015; McKee et al., 2009; Perez et al., 2013), but there are no comprehensive tests of this association. The present study addresses this proposition directly: that capillary degeneration gives rise to neurofibrillary degeneration in AD.

An initial step in testing this hypothesis is to determine the anatomical relationship between microvessels and the neuritic component of the plaque across the spectrum of neuritic disease stages. With this aim, we determined the location of NPs along the microvascular network and examined whether NPs colocalize with markers of hemorrhage and microvascular compromise. We present evidence that the neuritic component of the plaque arises from small hemorrhages, on the order of 50–200 μm, around microvessels. Linking neuritic degeneration to these microstrokes can provide a unifying hypothesis for the vascular etiology of AD.

2. Materials and methods

2.1. Case selection

This study was approved by the Human Research and Ethics Committee, University of Sydney. Tissue blocks were obtained from the Australian Brain Bank Network for Mental Health Research and the Victorian Brain Bank. Brains were immersion-fixed at autopsy in neutral buffered formalin. AD cases were diagnosed with dementia according to the consortium to establish a registry for Alzheimer's disease criteria (Morris et al., 1994) and diagnoses confirmed postmortem. Cases for this study (Table 1) were chosen to represent the spectrum of neurofibrillary pathology from Braak stage 0 to stage VI, according to neuritic staging criteria (Braak and Braak, 1991). The abundance and distribution of neurofibrillary tangles were used to determine the neuropathological stage for each case using tau and Aβ immunohistochemistry and Bielschowsky silver staining of 50-μm sections from medial temporal lobe (MTL) (hippocampus and entorhinal cortex), cingulate, and superior frontal cortices. Nondemented controls (NDCs) had no history of dementia and showed low to moderate neuritic pathology (stage 0–III). Stage 0 NDC cases were below threshold for scoring but did show scattered Hp-tau neurites and tangles and occasional early dystrophic neuritic clusters across the regions sampled. Mild AD dementia cases showed early cognitive symptoms and stage III–IV neuritic pathology at *postmortem*. Down syndrome (DS) cases with AD (DS/AD) were included as perivascular plaques, and microhemorrhages have been demonstrated in these cases (Cullen et al., 2005, 2006). Early neuropathological stage NDC, AD, and DS cases were of particular interest to this study as the lower density of lesions and lesser cortical atrophy, scarring, and tissue remodeling allowed a clearer view of neuritic plaque lesions in relative isolation.

2.2. Tissue processing

Blocks of formalin-fixed tissue were taken from the MTL (hippocampus and entorhinal cortex), fusiform, inferior, and superior temporal gyri and anterior cingulate and superior frontal cortices. From each block, serial 50- to 200-μm sections were cut using a CO_2 Leica microtome (Leica SM2000R) and collected into 0.1 M Tris buffer (pH, 7.4).

Tissue sections were labeled with markers for blood vessels: lectin *Ulex europaeus agglutinin* for endothelial cells (UEA lectin, biotin conjugated, 1:100, Vector Laboratories Cat# B-1065, RRID:AB_2336766) or collagen IV (1:100 Abcam Cat# ab6586, RRID:AB_305584) for endothelial basement membrane. The marker AT8 (1:1000, ThermoFisher Scientific Cat# MN1020, RRID: AB_223647) was used for Hp-tau neurofibrillary lesions. Free-floating sections were processed in Netwell cell culture inserts (Costar Corning) and then transferred to 5-mL vials for antibody incubations over 24–72 hours at 4 °C. Bound antibody was visualized using species-specific biotinylated secondary antibodies (Merck Millipore) and avidin-biotin complex (ABC elite, peroxidase- or alkaline phosphatase-linked, Vector Laboratories). Selected sections were counterstained with Cresyl violet for cell nuclei and Nissl substance. For immunofluorescence, sections were incubated in Alexa-linked species-specific secondary antibodies or streptavidin (Molecular Probes, Invitrogen) over 24 hours.

As a marker for microhemorrhage, a modification of the classic potassium ferrocyanide histochemistry was used to detect iron in free-floating thick sections with minimal background. For this Prussian blue (PB) staining, sections were prepared as for

Table 1
Cases details

Case	Dementia diagnosis	Sex	Age (y)	PMD (h)	B&B stage	Cause of death
NDC1	None	M	71	24	0	Bronchopneumonia
NDC2	None	M	84	48	0	Cardiac arrest
NDC3	None	F	92	24	I	Perforated gastric ulcer
NDC4	None	M	98	10	I	Pneumonia
NDC5	None	M	64	8	II	Cardiac arrest
NDC6	None	F	78	8	II	Cardiac arrest
NDC7	None	M	75	24	III	Cardiac arrest
AD8	mAD	M	81	3	III	Cardiac/respiratory arrest
AD9	mAD	F	76	8	IV	Respiratory arrest
AD10	mAD	F	83	24	IV	Cardiac arrest
AD11	mAD	F	73	24	IV	Sepsis
AD12	AD	M	67	20	V	Bronchopneumonia
AD13	AD	F	70	15	V	Atherosclerosis
AD14	AD	M	76	18	V	Bronchopneumonia
AD15	AD	F	58	7	VI	Bronchopneumonia
AD16	AD	F	63	5	VI	Cardiac arrest
AD17	AD	M	64	24	VI	Bronchopneumonia
AD18	AD	M	84	24	VI	Pneumonia
DS19	DS	F	25	24	0	Cardiac arrest
DS/AD20	DS/AD	M	54	24	III	Cardiac arrest
DS/AD21	DS/AD	M	58	57	III	Terminal seizure

Key: NDC, nondemented control; AD, Alzheimer's disease; mAD, mild AD; DS, Down syndrome; PMD, postmortem delay; B&B, Braak and Braak neuritic stage (0–VI).

immunohistochemistry and then incubated in plastic vials at room temperature in freshly prepared 4% potassium ferrocyanide in 2% HCl containing 0.01% Triton-X, for 72 hours at room temperature. Lectin UEA histochemistry or fluorescence immunolabeling for Hp-tau or collagen IV followed iron staining after thorough washes in Tris buffer.

2.3. Image capture and analysis

For bright-field microscopy, a Leica DMLB microscope fitted with a Jenoptik C14 camera and ProgRes software (V.14) was used. For epifluorescence microscopy, we used a Zeiss Axioimager 2, fitted with a motorized XYZ stage, an HRm camera and AxioVision software. Zeiss zvi files were imported into the Fiji application https://imagej.net/Fiji (Schindelin et al., 2012) for image processing and analysis.

2.4. Question 1: Are Hp-tau neurites in NPs located around capillaries?

In the first-pass qualitative and quantitative analyses, 50-μm sections labeled with UEA lectin and Hp-tau from 21 cases with stages 0-VI (Table 1) were examined. In each case, the intersection between microvessels and NPs was assessed in the MTL, fusiform, inferior, and superior temporal gyri and anterior cingulate and superior frontal cortices. NPs were selected for analysis by systematically stepping the microscope stage along an XY grid, from a random start, across the cortical ribbon or hippocampal sectors using a 20× objective. Even in 50-μm section, up to 10× the thickness of typical histological samples, most plaques with dimensions typically between 50 and 150 μm, would be tangentially sectioned, missing the central microvessel. Consequently, we then scaled up the analysis to thicker sections, 100–200 μm tissue sections coimmunolabeled for collagen IV and AT8 from 16 cases: 3 NDC, 11 AD, 2 DS/AD neuritic stages II–VI. Using a 20× objective, the microscope stage was stepped in the XY plane, from a random start, until at least 1 cluster of enlarged dystrophic neurites (the NP) was contained within the field of view (FOV). Stacks of optical z-planes were then captured through the full depth of the NP, with z-plane intervals of 1-μm, XY FOV dimensions 448 × 335 μm, and image resolution 1388 × 1040 pixels. NPs were considered only when the entire neuritic cluster was contained within the Z-stack. Sections were scanned through the full depth of each NP and scored on the basis of presence or absence of a capillary within the sampled plaque. A positive score required that NP neurites encircle a cross-section or longitudinal segment of a blood vessel. At least 10 FOVs were considered for each case, with at least 30 NPs assessed, except in cases DS/AD20 and DS/AD21, where only 20 whole plaques could be located within the section planes. Image capture and analysis were performed by separate observers, and all scoring was performed by 2 observers.

2.5. Question 2: Do NPs colocalize with markers of microhemorrhage?

We determined the colocalization of NPs with markers of microhemorrhage, such as iron and endothelial debris. All cases and sections were assessed in 50- to 200-μm sections labeled for Hp-tau, blood vessels, and iron.

2.6. Question 3: Are capillaries within the NP compromised?

To test whether vessels within NPs are compromised, we measured the difference in blood vessel diameter within a cluster of dystrophic neurites (NP) compared with the same vessel distal to the sampled NP. Whole NPs were acquired in randomly selected FOVs in 100- to 200-μm MTL, inferior and superior temporal sections from 7 cases (1 NDC and 4 AD and 2 DS/AD cases, stages III–VI) labeled for collagen IV and Hp-tau. Z-stacks were captured through the full depth of each NP, with step intervals of 1-μm, FOV 448 × 335 μm, image resolution 1388 × 1040 pixels. A minimum of 10 FOVs per section were examined. NPs were considered for analysis when the entire neuritic cluster of the NP was contained within the section depth. Fewer NPs were assessed in this question because of the more stringent requirement for sufficient lengths of blood vessel to be present both within and distal to the NP. Z-stack files were imported into the application Fiji to measure vessel diameters. The diameter of the vessel at the center of the NP (inside) and the diameter of the vessel at 50-μm from the perimeter of the NP (outside) were measured. For the vessel diameter "inside" the NP, each FOV was scrolled through the Z-stack until the vessel within the NP was in sharp focus. Using the line tool in FIJI, a line parallel to the vessel was drawn and a second line drawn across the vessel segment, perpendicular to the vessel axis to measure the cross-sectional diameter. This process was repeated for the vascular segment 50 μm from the NP perimeter to obtain the "outside" diameter. Measurements were made only when both the NP and central microvessel were contained within the section planes. Where NPs appeared at branch points, 2 vessels were typically involved. In this instance, the diameter of the uppermost vessel in the z-stack was measured.

2.7. Statistical analyses

The application Prism (v.7 GraphPad) and "R" (R Core Team, 2015) were used for statistical analysis. Data are expressed as mean ± standard deviation. A one-way ANOVA was used to test for vessel/NP association and vessel diameters between cases, dementia groups, and neuritic disease stage. A paired *t*-test was used to test the relationship between the vessel diameter inside and outside NPs in each case. A D'Agostino and Pearson omnibus normality test was performed to test for a Gaussian distribution of data. To determine the effect size of vessel narrowing, eta-squared (η^2) was calculated.

2.8. Three-dimensional rendering of the microvascular-NP spatial relationship

The Imaris application (Bitplane, v8.1.2, Zurich, Switzerland) was used to produce three-dimensional renderings of the NP relationship to microvessels in 200-μm tissue sections immunolabeled for collagen IV and Hp-tau (AT8). For each of the 3 cases (ND7, AD9, and AD17) used in these reconstructions, optical Z-stacks of five NPs were acquired at a resolution of 1388 × 1040 pixels, FOV 448 × 335 μm, 20×objective, with optical z-planes taken at 0.5-μm intervals. Z-stack files were processed in Fiji for bleach correction to normalize the brightness across optical z-planes, followed by the "find edges" tool to remove scattered light in 3 dimensions. Out of focus images at the top and bottom of the optical stack were removed. In IMARIS, surface renderings were generated using the manual surface creation tool to create a topographical contour map for three-dimensional rotatable images of microvessels and NPs.

3. Results

3.1. Question 1: Are Hp-tau neurites in NPs located around capillaries?

In this question, we tested the anatomical relationship between the Hp-tau neuritic component of the plaque and microvessels. A

consistent, nonrandom association of Aβ deposits with blood vessels in 50-μm sections from AD and plaque-positive controls has been previously demonstrated (Cullen et al., 2006). Tissue sections (50-μm), colabeled with UEA lectin histochemistry and Hp-tau (AT8) immunohistochemistry, showed cleanly labeled microvessels and Hp-tau dystrophic neurites in hippocampus, temporal, cingulate, and superior frontal cortices of all NDC, AD, and AD/DS cases. Although the density of NPs differed substantially between cases and brain regions, the morphology of neurites in NPs included punctate, bulbous, and thread-like Hp-tau–positive structures in all disease stages. In early neuritic stage cases, including NDC, AD, and DS/AD, NPs were scarcer by definition, particularly in cortical areas outside the MTL. In these early-stage cases, Hp-tau neurites in plaques appeared against a lesser interference from neuropil threads in the surrounding cortex, providing a distinct view of the perivascular arrangement of NPs in isolation (Fig 1). In areas of low NP density, particularly in early-stage cases, Hp-tau neurites encircled capillary segments with few neuropil threads outside the plaque area (Fig. 1A–F). In early stage, NPs cells with a compact heterochromatin, indicative of infiltrating granulocytes and macrophages and resident microglia, were interspersed with Hp-tau neurites, with astrocytic nuclei in the plaque periphery (Fig 1A and B). Perivascular clouds of lectin-labeling, indicative of damaged microvessels, were frequently interspersed with Hp-tau–positive neurites in NPs (Fig. 1C–E), as noted previously for Aβ and vessel colabeling (Cullen et al., 2005).

The perivascular focus of neurites comprising NPs remained consistent in mid- to late-stage (stages IV–VI) cases (Fig 2). In optical sections through the depth of whole NPs, the encircling of capillary segments by Hp-tau neurites was visible against a denser background of fine Hp-tau neurites in the neuropil (Fig. 2A–F). As in early-stage cases, this concentration of NP neurites around

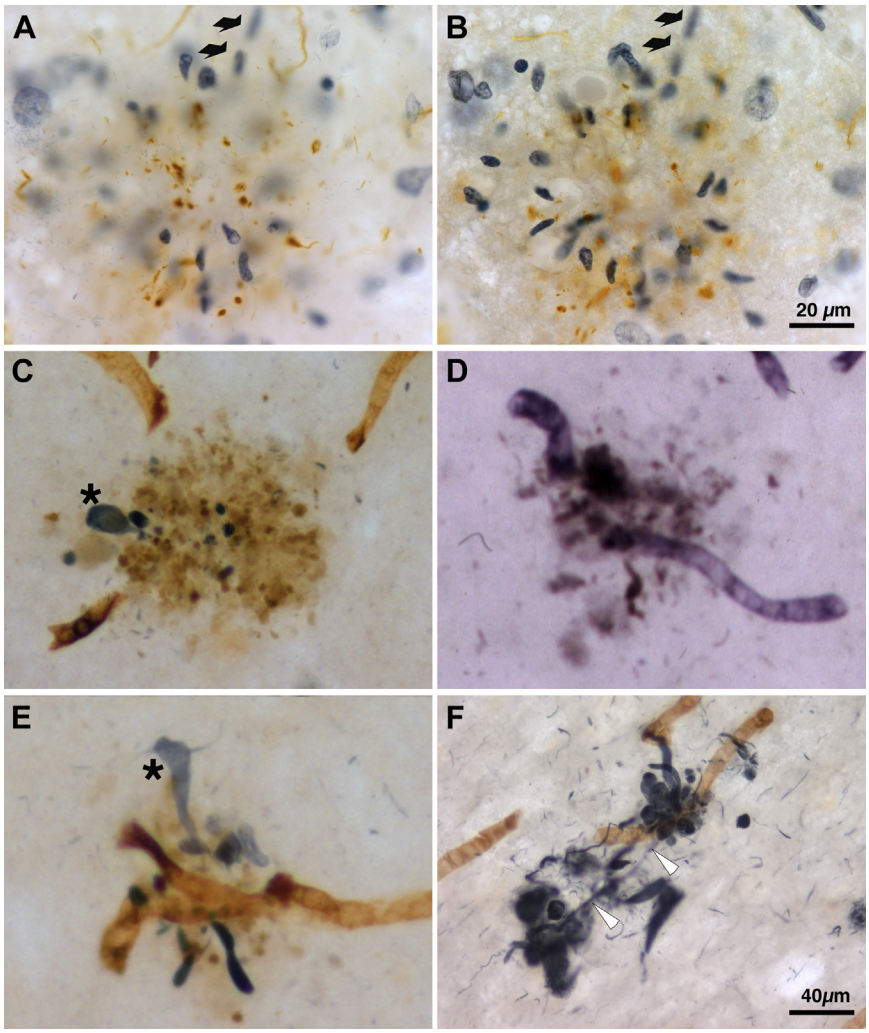

Fig. 1. Perivascular Hp-tau in cases with early-stage neuritic pathology. In early-stage plaques, dystrophic neurites in NPs can be seen surrounding microvessels, in relative isolation, with minimal neuritic threads in the surrounding neuropil. (A and B) An early NP is shown in 2 optical planes from a 50-μm section of the superior frontal cortex, stage III case NDC7 labeled for Hp-tau (AT8, brown) and Cresyl violet counterstain (blue). The plaque area is demarcated by the neuritic component, cell nuclei, and optical density differential. In this NP, Hp-tau–positive punctate structures radiate from a central capillary identified by tracking the elongated morphology of endothelial cell nuclei (arrows) through the plaque area. The neuritic puncta in this plaque are interspersed with cell nuclei showing a compact heterochromatin indicative of granulocytes, macrophages, and resident microglia, with astrocytic nuclei in the plaque periphery. (C-F) 50-μm Cortical sections Braak stage II cases NDC5 (C) and NDC6 (D) Braak stage III cases NDC7 (E), and AD8 (F) labeled for Hp-tau and lectin UEA. (C-E) Punctate and bulbous neuritic Hp-tau structures are closely focused around microvessels against a sparse background of scattered neuritic threads. (C and E) Endothelial debris, evident as a cloud of particulate staining around capillary segments (brown), is intermingled with early-stage Hp-tau neuritic structures (blue/black). In panel (D), UEA lectin for endothelial cells is shown in blue, with Hp-tau in brown/black. Panel (F) shows the tight clustering of enlarged neuronal structures around capillaries. Hp-tau neurites outline the path of a tangentially sectioned capillary segment (arrowheads). Occasional neurofibrillary tangles can be identified in the plaque periphery (asterisks in C and E). Scale bar = 20 μm (A–E), scale bar = 40 μm (F). Abbreviations: Hp-tau, hyperphosphorylated tau; NPs, neurite-containing plaques; NDC, nondemented controls; UEA, Ulex europaeus agglutinin. (For interpretation of the references to color in this figure legend, the reader is referred to the Web version of this article.)

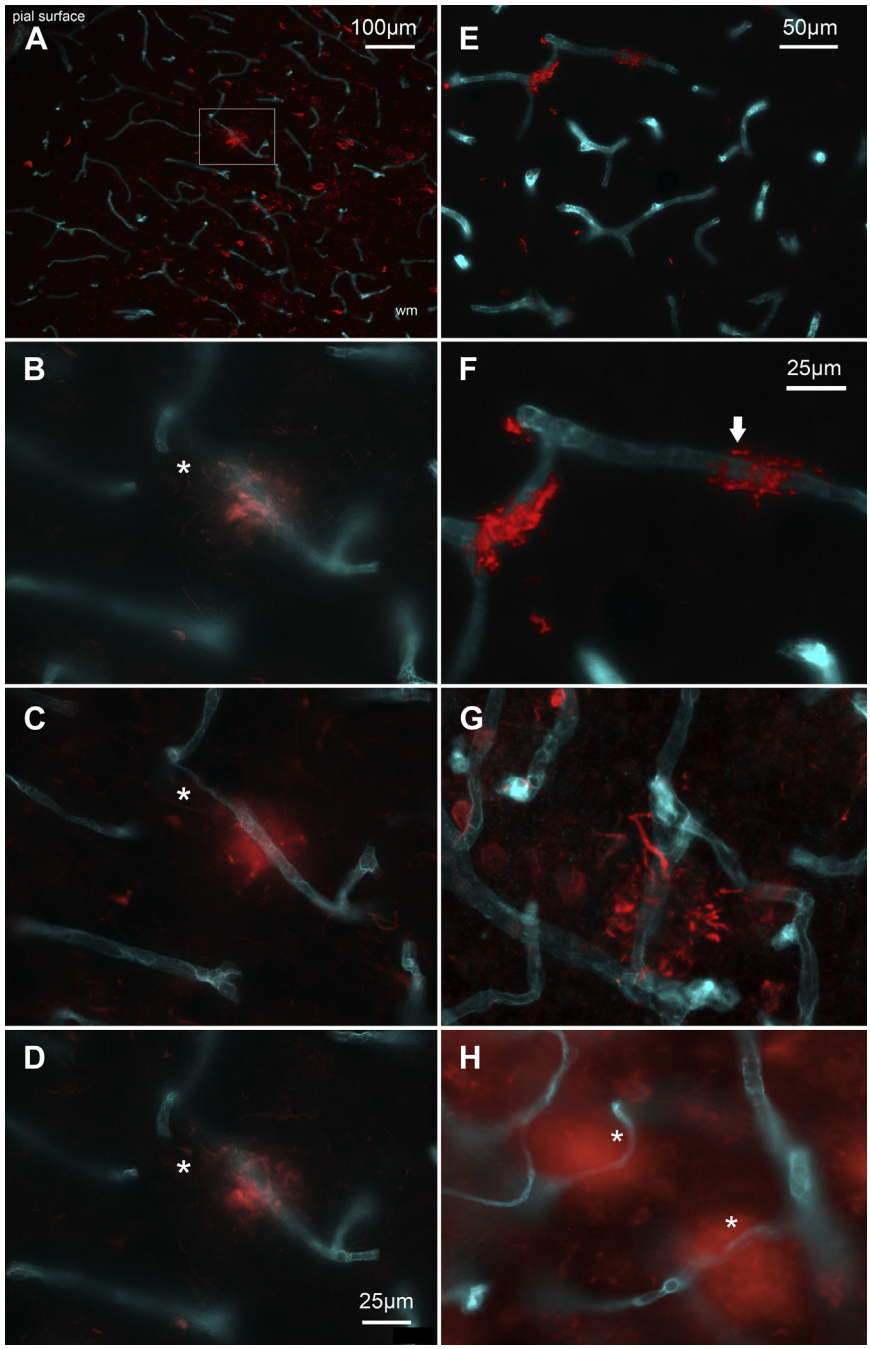

Fig. 2. NPs surround capillaries in cases with mid- and late-stage neuritic pathology. (A–F) Hp-tau (AT8, red), collagen IV (cyan). (A–D) Cingulate cortex, case AD15 (stage VI), 50-μm section. (A) Low magnification view of the cortical depth shows scattered NPs against finer caliber neuritic threads and tangles. The NP (box) in the center of the FOV is fully contained within the section thickness (B–D). (B–D) Three optical section planes through the depth of this NP show Hp-tau–positive neurites of the plaque surrounding the capillary segment. The involved capillary is significantly narrowed at the edge of the NP domain (asterisk). This collapsed "string vessel," with a diameter of less than 2 μm, indicates a substantially restricted blood flow in the microlocal plaque area. (E and F) Cingulate cortex, 100-μm section, stage IV case AD9. At lower magnification (E), there is a conspicuous focus of Hp-tau neurites around capillary segments. At higher magnification (F), the close anatomical relationship between these neurites and microvessels is striking. A cross-section of a capillary branch, perpendicular to the plane of section, is indicated by an arrow (F). Hippocampal 150-μm sections from stage IV case AD9 (G) and stage VI case AD17 (H). A greater number of NPs is present in these later stage cases, with a denser background of neuritic threads extending into the adjacent neuropil. As in earlier stage cases, NPs are focused around capillaries. Collapsed microvessels within the NPs in are indicated (asterisk). Scale bars (A) = 100 μm; (B–D) = 25 μm; (E) = 50 μm; (F–H) = 25 μm. Abbreviations: Hp-tau, hyperphosphorylated tau; NPs, neurite-containing plaques; FOV, field of view; wm, subcortical white matter. (For interpretation of the references to color in this figure legend, the reader is referred to the Web version of this article.)

microvascular segments remained consistent in areas of high-density neuropil threads and greater NP numbers (Fig. 2G and H). There was conspicuous narrowing of microvessels within and adjacent to the focus of neurites in the plaque, frequently extending to a nonpatent, collapsed vessel (asterisks, Fig. 2B–D, H).

The location of NPs along the microvascular network was quantified to test the frequency with which plaques encircle capillaries. In the first-pass analysis, UEA lectin–labeled and AT8-labeled 50-μm sections from the hippocampus and entorhinal area (MTL), temporal, cingulate, and superior frontal neocortices were assessed in 21

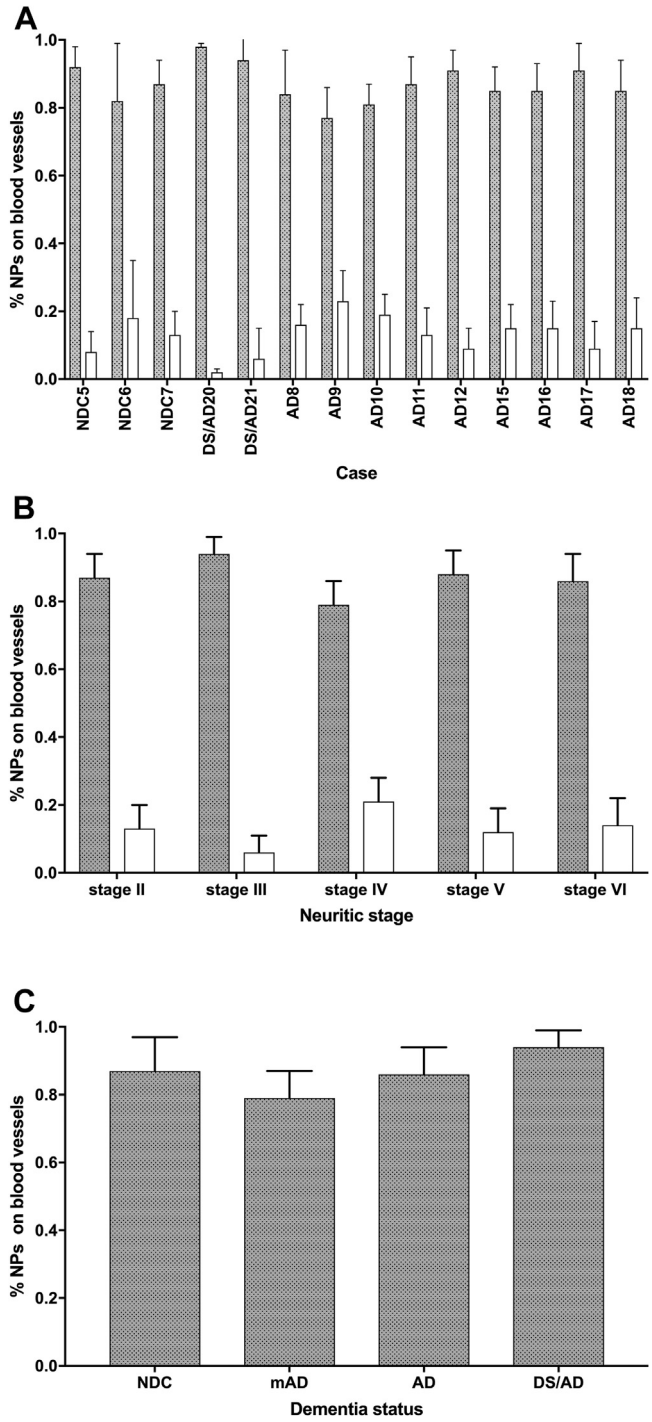

Fig. 3. NPs are perivascular independently of case, dementia, or neuritic disease stage. The intersection between NPs and capillaries was quantified by (A) case, (B) Braak neuritic stage, and (C) dementia diagnosis. Gray bars represent the percentage of NP containing an intersecting capillary (positive score), with white bars showing sampled NPs containing no capillary segment (negative score). Whole NPs in each field were scored in 100- to 200-μm sections from hippocampus, entorhinal cortex, superior and inferior temporal lobes. Ten FOVs considered for each region in each case and at least 30 whole NPs were scored for the plaque/microvessel intersection, except in DS cases where only 20 whole NPs were present in the samples. Data are expressed as mean values ± standard deviation. (A) By individual case, the NP association with blood vessels ranged from 77% to 97%, mean 87 ± 5.7%, across all cases. There was no significant difference in the NP/microvessel association between cases ($p > 0.99$). The NP/microvessel association did not differ significantly by (B) neuritic stage, $p > 0.99$, (F, 0.0036; R^2 0.0029) or (C) clinical group (AD, mAD, NDC, DS) $p > 0.99$ (F, 0.0045; R^2 0.0033), one-way ANOVA. The consistent anatomical relationship between NPs and microvessels, independent of neuritic burden and dementia diagnosis, suggests a common microvascular origin for NP development. Abbreviations: NPs, neurite-containing plaques; FOV, field of view; AD, Alzheimer's disease; mAD, mild AD; NDC, nondemented controls; DS, Down syndrome.

NDC, AD, and DS cases. A microvessel within the NP cross-section was required for a positive score. In 50-μm sections, there was a 71%–95% positive intersection of NPs with blood vessels across all cases and brain regions. This association of NPs and microvessels did not differ significantly by individual, neuritic stage, cognitive status, AD diagnosis, age at death, or brain region ($p > 0.99$).

As the full dimension of most NPs cannot be captured even within 50-μm tissue sections, and less so in more typical 7–10 μm sections, we scaled up to 100–200 μm sections to assess the NP/microvessel association using the more stringent requirement for a vessel to be present within the perimeter of a whole neuritic cluster entirely contained within the section planes. In all cases, NDC, AD and DS, a microvessel segment was present in 77%–97% of NPs (mean 87 ± 5.7%). In 5 cases, this association was greater than 90% (Fig. 3A). The spatial relationship between microvessels and NPs did not differ significantly by neuritic stage ($p > 0.99$; F, 0.0036; R^2, 0.0029) or clinical diagnosis ($p > 0.99$; F, 0.0045; R^2, 0.0033) (Fig. 3B and C). There was a small inverse correlation between age and NP/blood vessel association ($p < 0.005$; F, 14.6; R^2, 0.6098). Together, these data demonstrate that NPs encircle microvessels with high frequency across disease stages and independently of dementia diagnosis.

3.2. Question 2: Do NPs colocalize with markers of microhemorrhage?

PB labeling of free-floating sections was followed by immunolabeling for Hp-tau or collagen IV for blood vessels. In NPs, iron-positive deposits were interspersed with Hp-tau neurites around a central microvessel (Fig. 4A–D). Hp-tau neurites surrounded microvessels through the depth of the NP, with an iron-positive core in line with the capillary lumen (Fig 4A–D). Hp-tau neurites of the NP surround an iron-positive core and are interspersed with iron-positive neurites (merged image Fig 4D). In the cross-section, this wrapping of small vessels by dystrophic neurites, with a halo of Hp-tau neurites radiating from a dense iron or hollow core (Fig. 4D and E), reflects the classic view of a plaque seen in typical thin-section neuropathologic analysis. Neurons and tangles containing iron were present within and around the NPs domain (Fig. 4E and F). In fortuitous sections, iron-positive puncta could be traced from a neuronal cell body through a neurite ending on a microvessel (Fig. 4F).

3.3. Question 3: Are capillaries within the NP compromised?

We next asked whether NPs contained evidence of compromised blood vessels by measuring microvascular diameters inside and outside NPs in 100- to 200-μm sections. The mean microvessel diameter was significantly narrowed within the NP compared with vessel segments outside the NP domain in all cases ($p < 0.001$; 2-tailed t-test). A reduced microvascular diameter within NPs was seen in all cases, neuritic disease stages, and NDC, AD, and DS/AD groups (Fig. 5A–C). The extent of vessel narrowing differed between cases, with the most striking vessel narrowing seen in late stage V and VI AD cases (Fig. 5C). Vessels narrowed to less than 4 μm (boxed area Fig 5A) can be expected to result in compromised normal local blood flow. Vessel narrowing frequently extended to a full collapse of the microvessel to a nonpatent diameter of less than 2 μm (Fig. 5A), essentially a string vessel composed of extracellular matrix basement membrane without a viable endothelial cell layer (Fig. 2B–D, asterisks) (Challa et al., 2002). Cases with more severe neuritic involvement (stages V and VI) had a significantly greater

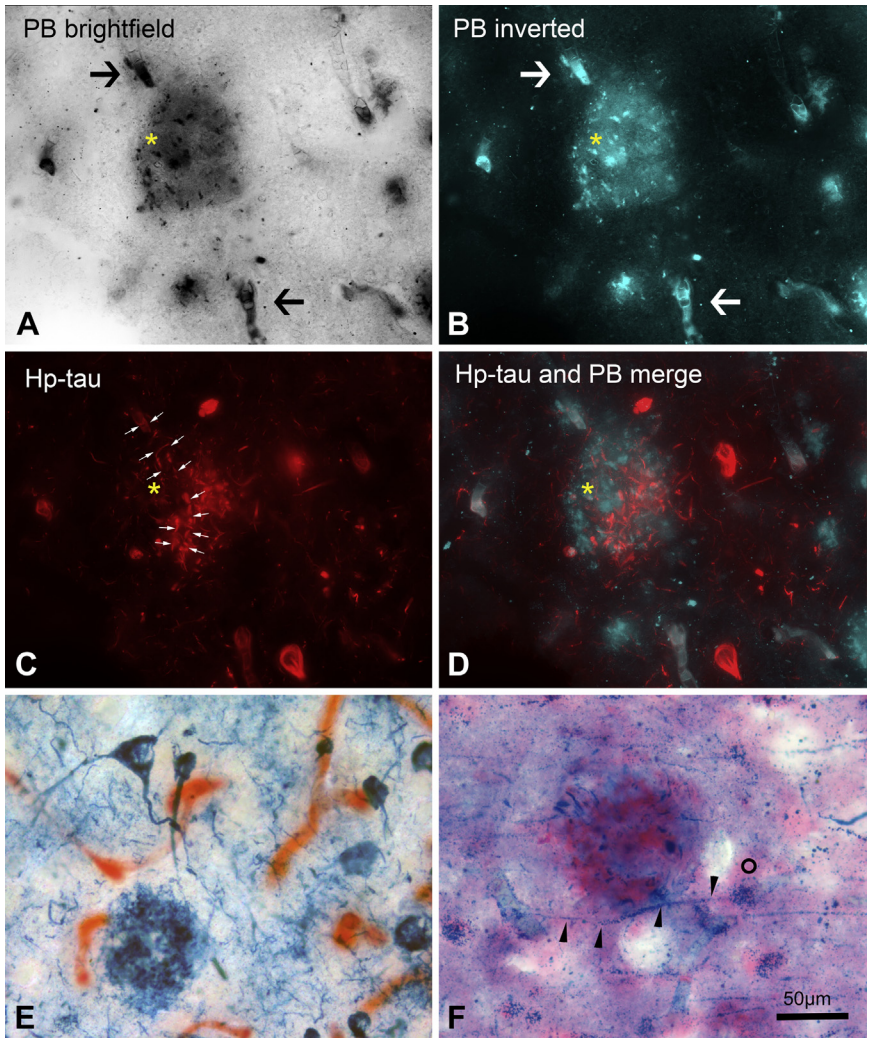

Fig. 4. NPs coincide with iron deposits and iron-positive neurites. (A–D) Representative NP in a 50-μm section of the cingulate cortex, case AD17 (stage VI), stained with Prussian blue (PB) for iron and immunolabeled for Hp-tau. Panel (A) shows a view of PB staining captured in bright field, with the inverted pseudocolored (cyan) image in panel (B). Fragments of an iron-stained microvessel can be tracked through the central NP (large arrows, A and B), with an iron-positive core (asterisk) in-line with the path of the capillary. A halo of iron-positive neurites within the diffuse iron deposit can be seen within the plaque area. (C) Hp-tau immunostaining (red). A ring of Hp-tau neurites radiates from the center of the NP against a background of finer neurites. HP-tau neurites border a capillary (unstained) traversing the NP (C, small arrows), with tangles scattered in the periphery of the NP. In the merged view (D), Hp-tau neurites of the NP can be seen surrounding an iron-positive core (asterisk) and are interspersed with iron-positive neurites. This view of iron/Hp-tau staining resembles the classic NP picture, with a dense core center surrounded by a halo of dystrophic neurites. (E) Bright-field image of a 50-μm hippocampal section from case AD15 (stage VI), labeled for iron (PB) and blood vessels (lectin UEA, magenta). In the center field, an NP appears against a background of finer caliber, iron-positive neurites and scattered neurofibrillary tangles in the periphery. (F) NP in 50-μm hippocampal section from case NDC7 (stage III), stained for iron (PB) and then immunolabelled for Hp-tau (magenta). Hp-tau neurites, diffusely stained with the alkaline phosphatase reaction product, are interspersed with iron-positive fibers in the NP. Iron is also localized to a neuronal soma (circle), with an iron-positive process (arrowheads) ending on a length of an iron-positive capillary. Scale bar = 50 μm (A–F). Abbreviations: Hp-tau, hyperphosphorylated tau; NPs, neurite-containing plaques; NDC, nondemented controls; UEA, Ulex europaeus agglutinin. (For interpretation of the references to color in this figure legend, the reader is referred to the Web version of this article.)

proportion of within-NP vessels in this severely constricted range (Fig 5A). Case DS/AD21 (stage III) was distinctive, with microvessels both within and outside NPs larger on average than in other cases assessed; however, there was a relatively reduced within-NP vessel diameter, consistent with observations in other cases.

To gauge the functional effect size of vessel narrowing within the NP, the η^2 statistic was calculated to predict the relative difference in vessel diameters [(outside-inside)/outside], with neuritic disease stage as a fixed effect. There was a large effect size in all pairings for each case (η^2 0.50–0.80), controlling for the effect of age and postmortem interval (adjusted $R^2 = 0.22$, $F(6, 125) = 7.27$; $p < 0.001$). In this model, increasing neuritic disease severity is associated with a greater reduction in capillary diameter within the NP ($p < 0.001$) (Fig. 5B). Over the cortical and hippocampal distribution of NPs, the average reduction in vessel capacity (Fig. 5C) between 16% and 65% can be expected to result in a markedly decreased cerebrovascular perfusion. Microvessels have a narrow range of patency. An important biological implication of these effect sizes is that even small diameter differences can substantially reduce normal microlocal perfusion.

For a three-dimensional view of the spatial association of Hp-tau plaques and microvessels, 200-μm sections of hippocampus, labeled for collagen IV and Hp-tau, were used to capture a more extensive portion of the microvascular architecture alongside NPs. In a series of optical sections, the wrapping of capillaries by enlarged Hp-tau neurites can be seen through the full depth of the NPs (Fig. 6A–C). In these views, NP-associated capillaries are seen feeding from a single arteriole, identified by the smooth muscle banding and vessel diameter (Fig. 6A–C). One NP in this view (marked *** in Fig. 6A–C) would not have been counted as having a

central vessel for the NP/vessel association analysis (question 1, Fig. 4.); however, a stub of a capillary and the path of the microvessel can be seen tracking through the depth of the plaque (Fig. 6C arrow and Supplementary Figure). With microvascular pathology including frank rupture or collapse, it is not surprising to find that sufficient lengths of NP-associated microvessels were not sufficiently intact for detection in histology. The surface rendering in Fig. 6D shows the specific anatomical relationship between NPs and microvessels. The striking arrangement of NPs around capillaries is a strong indication of a link between the formation of plaques and events at the microvascular interface. For the full optical stack of the NPs in Fig. 6, see the Supplementary Video.

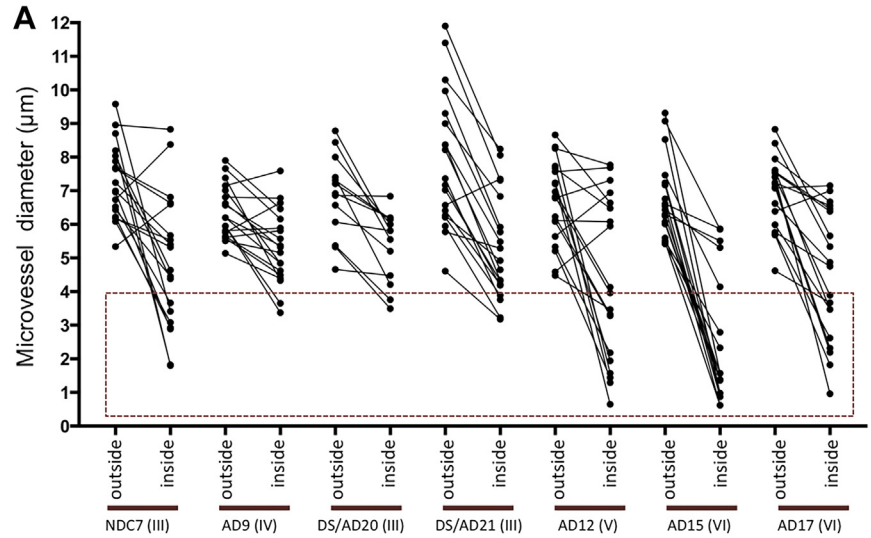

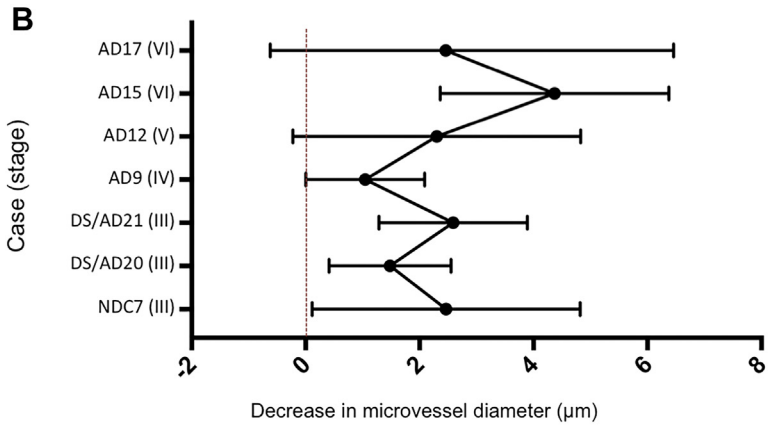

C

Case	Stage	Outside NPs	Inside NP	Mean Δ	Relative Δ
NDC7	III	7.22±1.07	4.75±1.96	- 2.46±2.29	-0.34
DS/AD20	III	6.99±1.23	5.22±1.05	- 1.82±1.07	-0.22
DS/AD21	III	7.90±2.00	5.31 ±1.59	- 2.59±1.30	-0.33
AD9	IV	6.38±0.84	5.33±1.05	- 1.05±1.02	-0.16
AD12	V	6.67±1.18	4.37±2.32	- 2.30±2.46	-0.34
AD15	VI	6.74±1.10	2.37±1.81	- 4.37±1.96	-0.65
AD17	VI	6.87±1.06	4.41±1.88	- 2.46±1.79	-0.36

Fig. 5. Blood vessels are compromised within neuritic plaques. Microvascular diameters within NPs (inside) are reduced compared with diameters outside the plaque area. (A) Paired microvessel diameters outside and inside single NPs in 100- to 200-μm sections. Diameter pairs were measured from 20 whole NPs in each case, except for DS/AD20 (n = 19) and DS/AD21 (n = 13). The within-plaque capillary diameter was reduced compared with the capillary segment outside the NP domain in 95% of plaques assessed. In later stage cases, vessel narrowing was substantial, constricting the within-NP microvascular diameter below 4 μm (boxed area) and unlikely to support normal local blood flow. Notably in late-stage cases, microvessels within the NP frequently measured below 2 μm, essentially a collapsed nonpatent "string" vessel without a viable endothelial layer. (B) The mean difference in microvascular diameter inside/outside NPs. The average narrowing of microvessels within NPs ranged from 1.1 ± 1.0 μm to 4.4 ± 2.0 μm across cases, a relative reduction between 16% (AD9) and 65% (AD15). Bars show the range of narrowing in paired microvessel diameters. (C) Vessel diameters (μm) outside/inside NPs ± standard deviation. Δ = difference outside/inside, mean difference ± standard deviation. Relative difference is % mean vessel diameter outside compared with inside NPs. The relative difference is calculated as mean outside diameter/mean inside diameter. Over the cortical and hippocampal distribution of NPs, this average reduction in vessel capacity is likely to result in a marked reduction in cerebrovascular perfusion. Abbreviations: NPs, neurite-containing plaques; DS, Down syndrome; AD, Alzheimer's disease.

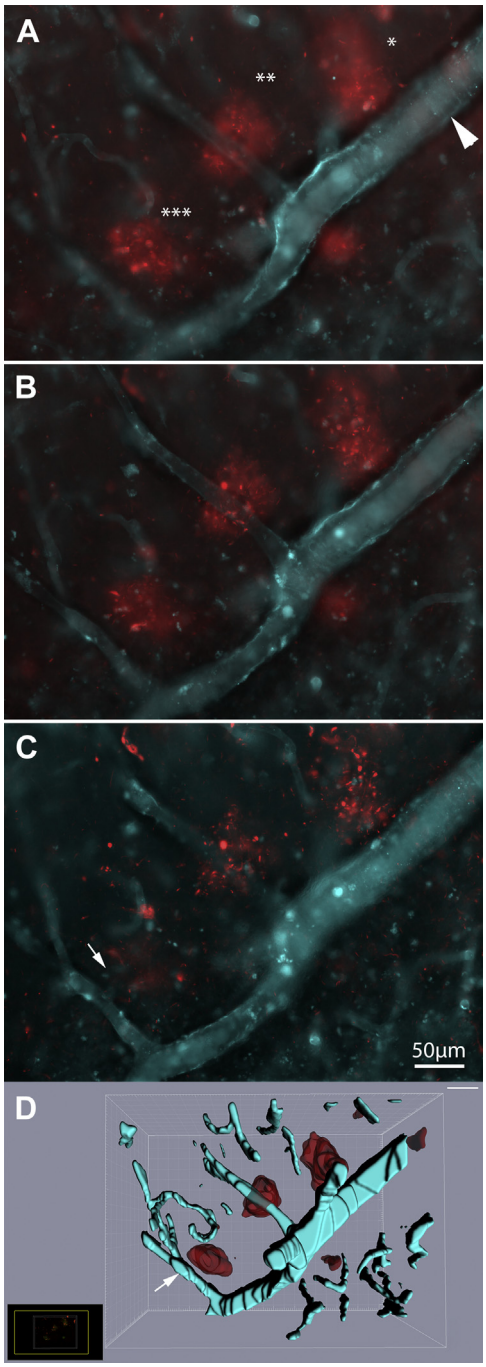

Fig. 6. Three-dimensional view of the spatial association between NPs and microvessels. (A-C) Three optical planes through a 200-μm section of hippocampus stage III case NDC7, collagen IV (cyan), and Hp-tau (AT8, red), showing three NPs wholly contained within the section planes. A z-stack of the 448 × 335 μm FOV was captured at 0.5 μm intervals using a 20× objective at a resolution of 1388 × 1040 pixels to provide a three-dimensional image through the full section depth. Three capillaries are involved, arising at 90° from a single arteriole, identified by the smooth muscle banding (arrowhead in A). The NPs marked (*) and (**) surround a capillary, with the third NP marked (***) surrounding a vessel stub and groove that can be traced through the NP (arrow in C). A complete series through the plaque marked (***) can be seen in the Supplementary Image. Full views of the z-stack can be seen in the Supplementary Video. Scale bar = 50 μm for (A–C). (D) A three-dimensional surface rendering of the field in (A–C) from a 200-μm section of the hippocampus, case NDC7, illustrates the direct anatomical relationship of NPs to microvessels, with neurites of the plaque concentrated around capillaries. Abbreviations: NPs, neurite-containing plaques; FOV, field of view; Hp-tau, hyperphosphorylated tau; NDC, nondemented controls. (For interpretation of the references to color in this figure legend, the reader is referred to the Web version of this article.)

4. Discussion

Fundamental questions in unraveling the pathogenesis of AD include whether Aβ deposition leads to neuritic derangement, Hp-tau pathology leads to deposition of Aβ, or these components arise in parallel by separate mechanisms. An alternative proposition is that Hp-tau neuritic pathology and Aβ deposition are downstream sequelae of an independent pathological mechanism: microvascular degeneration. We report a consistent spatial association between dystrophic neurites of the plaque and microvessels across neuritic disease stages, dementia diagnoses, and age. The current investigation complements previous work showing that the Aβ component of plaques is consistently perivascular and coincident with microhemorrhages (Cullen et al., 2005, 2006). The anatomical relationship between microvascular pathology, dystrophic neurites, and Aβ deposits supports a mechanistic link between the key plaque components and events at the microvascular interface.

4.1. Neuritic plaques are anatomically linked to the microvasculature

We find that dystrophic Hp-tau neurites of NPs are consistently focused around impaired microvessels across the spectrum of neuritic disease stages in AD, DS, and NDC cases. This pattern of NPs encircling microvessels is independent of dementia status or patient age. Cases with sparse lesions offered the greatest potential to test the link between the neuritic component of the plaque and microvessels. Mildly affected stage 0–III cases have a clearer, more unencumbered view of the NP and blood vessel association against a minimal background carpet of neurites. In these early neuritic stages, Hp-tau neurites are mainly confined to the immediate plaque domain, with punctate and enlarged bulbous processes radiating from a central capillary against a minimally affected parenchyma, suggesting that Hp-tau neurites of the NP are perivascular from the very earliest appearance of the plaque. In more advanced neuritic stages, despite a significantly denser meshwork of fine Hp-tau neuritic threads in the surrounding neuropil, plaque neurites can be reliably demarcated as perivascular focal collections of enlarged Hp-tau neurites.

4.2. Microvascular integrity is impaired within the neuritic plaque

The integrity of the microvasculature is compromised within the NP domain, demonstrated by reduced microvessel diameters, pericapillary endothelial debris, and microhemorrhage markers. Microvessels within NPs are consistently narrowed across all neuritic stages, most dramatically in cases with late stage (V and VI) neuritic pathology. In late-stage cases, the capillary lumen within NPs is frequently reduced below capacity to support normal microlocal blood flow, often frequently to collapsed nonpatent “string vessels” composed of a collagen basement membrane without an intact endothelium (Challa et al., 2002). Over the cortical and hippocampal distribution of NPs, the mean reduction in vessel diameter within NPs ranged between 16% and 65% compared with microvessels outside the plaque domain with diameters on the order of 7.9 ± 2.0–6.4 ± 0.8 μm. Within the tight range of microvascular capacity, small reductions in capillary diameter can have a profound effect on microlocal blood flow. As plaque density increases with disease progression and more extensive areas of cortex are involved, greater numbers of microvessels within NPs are compromised. Collectively, the accumulated diminishment of local microvascular blood flow within and around plaques would be expected to have a profound effect on cerebrovascular perfusion.

4.3. Methodological considerations

The present investigation is essentially an anatomical study and provides an updated three-dimensional view of the plaque. Using tissue sections of 50–200 μm, we were able to capture greater portions of NPs and microvessels for a more comprehensive view of the plaque and microvascular network. These preparations are 10- to 30-fold thicker than typical histopathology sections, capturing whole plaques with diameters typically in the range of 50–100 μm or greater. In thinner samples, the central vessel would not appear in most NPs as the cutting plane would be tangential to the capillary in most sections. Focusing through the entire NP in these thick sections, an updated three-dimensional perspective of the classic picture of the NP emerges, showing clusters of enlarged, bulbous, punctate, and thread-like Hp-tau neurites, radiating from a central capillary. From this view of the three-dimensional relationship between the microvessel and plaque components, several testable hypotheses emerge for the vascular origin of the plaque.

We find here that NPs are marked by iron deposition characteristic of microhemorrhage as previously shown for Aβ deposits (Cullen et al., 2005, 2006). Using a refinement of the classic potassium ferrocyanide method, we were able to detect iron with high sensitivity in thick tissue sections, with capacity for subsequent labeling for microvessels and Hp-tau. Iron-positive neurites are interspersed with Hp-tau neurites, with full profiles of iron-positive neurons with endings contacting microvessels. Lengths of blood vessels were also iron-stained, as noted with variants of the PB stain (Burdo and Connor, 2003; Koeppen et al., 1995). Halos of Hp-tau neurites surround capillaries and contain a central iron-positive core within or adjacent to the microvascular lumen. In early NPs, plaque neurites are interspersed with resident microglia and blood cells infiltrate, as might be expected from a disruption of endothelial integrity. Together, the alignment of microhemorrhage markers, cell infiltrate, and Hp-tau neurites around narrowed microvessels supports a mechanism for neurodegeneration in AD directly linked to microvascular compromise. Neurons containing iron and Hp-tau can be directly traced to endings on microvessels. Iron-positive tangles and neurites have been well-noted in histology (Connor et al., 1992; LeVine, 1997; Smith et al., 1997) and more recently using multispectral Raman imaging (Michael et al., 2017).

4.4. Mediators of neuritic damage within microhemorrhages

Plaques containing Aβ deposits and dystrophic neurites are classic lesions in the identification of AD and are common in lower density in late age. The current report analyzed the vascular relationship of the neuritic plaque component separately to Aβ deposits. We have previously shown, in the same case cohort, that Aβ deposits are perivascular and colocalize with microhemorrhages (Cullen et al., 2006). A detailed neuropathological analysis of plaques has demonstrated that not all Aβ deposits coincide with a neuritic component and most but not all neuritic plaques are Aβ positive (Furcila et al., 2018). The microvasculature links both these components of the plaque anatomically. The contribution of Aβ oligomers in promoting neuritic dystrophy within the senile plaque/microinfarct area cannot be discounted. Aβ peptides are among many potential mediators of neuritic damage in the microhemorrhage area.

Several mediators of neuritic damage are contained within the complex components of a microhemorrhage. These components have potential to act acutely and chronically to initiate and exacerbate local neuronal degeneration of cells and processes. The breach of a capillary, with a diameter less than 10 μm, introduces neurotoxic compounds into a very small demarcated area of the parenchyma. As noted in large vessel hemorrhage, this infiltrate would contain hemoglobin from lysed red blood cells (Garton et al., 2016; Lee et al., 2010; Yip and Sastry, 2000), unsequestered redox-active iron (Koeppen et al., 1995; Wagner et al., 2003), as well as the coagulation-related factors thrombin and fibrinogen (Cortes-Canteli et al., 2012; Suo et al., 2003).

Events within the microinfarct, such as microlocal hypoxia (Raz et al., 2019), blood-brain barrier disruption and release of unsequestered iron are candidate mediators of damage to perivascular neuronal processes and neurons within the microinfarct domain. Infiltration of resident and extrinsic immune cells, including microglia and macrophages, is a source of neurotoxins within the microinfarct, including glutamate and quinolinic acid (Guillemin et al., 2005), with direct effects on aberrant tau phosphorylation (Rahman et al., 2009). Excess iron has the potential to facilitate quinolinic acid production as a known cofactor in the activity of kynurenine pathway enzymes involved in its production (Stachowski and Schwarcz, 2012).

Elevated redox-active iron is a potential mediator in the development of AD lesions (Cristovao et al., 2016; Liu et al., 2018) and has been shown to promote tau phosphorylation and aggregation (Nübling et al., 2012; Rao and Adlard, 2018) as well as assembly of Aβ fibrils (Bush and Tanzi, 2008; Castellani et al., 2012; Liu et al., 2011; Moreira et al., 2005). Hemoglobin promotes Aβ oligomerization (Wu et al., 2004) and extravasated macrophages and platelets within microhemorrhages are also sources of Aβ production and consolidation (Chen et al., 1995; Pluta, 1997). In this light, that Aβ deposition may have a beneficial function as a sealant at the vascular interface is a productive hypothesis in the repair response to microvascular injury (Atwood et al., 2003).

Extrapolating from larger vessel infarcts, the microinfarct is also likely to be characterized by delayed neuronal death subsequent to local hypoxia (Park et al., 1996; Wu et al., 2002), sustained calcium dysregulation, glutamate elevation (Osuga and Hakim, 1994), excitotoxicity, and apoptosis (Nitatori et al., 1995). There are immediate gains to be made by systematic comparison of plaque microinfarcts with the extensive pool of data on the composition, timing, and resolution of larger vessel infarcts.

4.5. Microhemorrhage chronology and neuritic plaque development

Determining a chronology for lesion development in a static postmortem picture requires caution. Nonetheless, there are clues in the tissue and case profiles that can help to assemble a hypothesis for a sequence of events in the initiation and progression of perivascular neuritic dystrophy for testing in humans in vivo and in animal models. Cases with minor to moderate neuropathology below the threshold for AD diagnosis or in early stage disease present a valuable group for study. In these cases, there is a minor background of neuropil threads surrounding the NP and fewer tangles, plaques are scarcer, and the cortical cytoarchitecture is relatively intact with minor cortical atrophy, scarring, and tissue remodeling. In early-stage cases, we see that Hp-tau neurites are substantially confined to the pericapillary area. The punctate and bulbous Hp-tau neurites of recent plaques are interspersed with intact blood cells and endothelial debris. This active microinfarct region, around an impaired capillary, encompasses an area of about 100 μm, the size of a classic plaque. The relatively undisturbed parenchyma in these views of early NPs indicate that these are recently formed lesions, and that Hp-tau is present in terminals from the earliest time of the microvascular event, as evidenced by the presence of these blood cells transient in the living brain.

Determining the consequences of microhemorrhages in AD can borrow from established ideas about cellular and neurochemical mechanisms subsequent to large vessel strokes in human and animal models in which the origin, timing, and progression can be specified (Chen et al., 1993; Koeppen et al., 1995; Wagner et al.,

2003). The intraparenchymal blood cell component of infarcts has a predictable time course in the brain and is resolved within a few days (Koeppen et al., 1995; Wagner et al., 2003), suggesting that plaque microinfarcts observed here are likely to be locally active for a brief time. In contrast, the iron of hemorrhages is an indelible marker persistent over many years (Koeppen, 2003; Lee et al., 2010; Wagner et al., 2003). Microhemorrhages appear to occur chronically, as recent active lesions with a transient cell component appear alongside established, resolved lesions across brain regions and cases. Individually, these microinfarcts are small, with diameters of 50–150-μm, but collectively occupy as much as 9% of the cortical mantle in advanced AD stages (Cullen et al., 2006). Reduced microvascular capacity in the plaque domain, summed over the increasing density of neuritic plaques with disease advancement, can be expected to propel a cascade of hypoperfusion, neuronal degeneration, and AD pathology generally (Okamoto et al., 2012).

The whole of the neurovascular unit needs to be considered in the initiation and progression of the plaque (Benarroch, 2007). Neuronal processes within the NP are enlarged and bulbous, consistent with the picture of neuronal terminal damage as seen in whole animal and tissue culture models of neuronal injury (Chen et al., 2004; King et al., 1997). Neuronal processes from diverse sources, including afferent cholinergic, dopaminergic, serotonergic, noradrenergic, and glutaminergic subcortical and intracortical neurons are known to contact and wrap microvessels (Hamel, 2006), leaving perivascular neurites directly vulnerable in the microinfarct core and penumbra. In addition to the acute degeneration of neurons and neurites in the microinfarct, chronic changes would include degeneration of neuronal processes terminating on or near damaged microvessels, loss of innervation of small vessels along the microvascular network, and microhemorrhage reaction and resolution, including acute inflammation and longer term astrocytic scar formation (Cullen, 1997). Neurovascular coupling within the neurovascular unit at the level of the capillary and small arteriole adjusts microlocal blood flow in response to local neuronal activity and oxygenation (Attwell et al., 2010; Lecrux and Hamel, 2011). Deafferentation of microvessels potentially exacerbates microvascular dysfunction, reducing blood flow through microvessels, the site of oxygen and nutrient exchange. As the disease progresses and increasing numbers of within-NP vessels are impaired, the feed-forward effect of this hypoperfusion may be part of the cascade of perivascular neurodegeneration and reduced Aβ clearance. Progressive hypoperfusion has been noted in AD (De Jong et al., 1999; Thomas et al., 2015). Congophilic angiopathy and reduced Aβ clearance via the perivascular glymphatic system are candidates for precipitating microvascular impairment (Chen et al., 1993; Lee et al., 2010; Perez et al., 2013).

4.6. Building a model for perivascular neuritic degeneration in AD progression

A persistent unresolved question in understanding the progression of AD neuritic pathology is whether intraneuronal tangles represent retrograde degeneration from damaged terminals. Several elegant analyses have attacked the problem of complexity of local disease markers, plaques and tangles, superimposed on the complexity of brain connectivity (Mesulam, 2000; Schönheit et al., 2004; Yilmazer-Hanke and Hanke, 1999) to explain the distribution of plaques and tangles. In direct analyses, neurites have been traced to tangle-laden neurons (Braak and Braak, 1988). Generalizing these observations to all tangles is an impractical task in human postmortem studies, given the high density of Hp-tau neurites in AD and the anatomical complexity of intracortical and subcortical connections. The findings from the present study can contribute to this debate and support a mechanism of neuronal degeneration radiating from axonal terminals on or near compromised microvessels, neuronal processes in passage and local neuronal cell bodies within the microhemorrhage. Our observations suggest an acute neuronal terminal swelling and tau hyperphosphorylation within the plaque microinfarct area, appearing within days of microvascular breakdown. Based on this scenario, the acute phase of the microinfarct is followed by a sequela of sustained retrograde and anterograde degeneration from the point of injury.

We propose a theoretical mechanism that relates microvascular degeneration to the progression of brain-wide neuritic pathology in AD, consistent with the apparent progression of neuritic pathology along cortical circuitry in AD (Mesulam, 2000; Schönheit et al., 2004; Yilmazer-Hanke and Hanke, 1999). In this model, neuronal processes terminating on or near microvessels would be most vulnerable within the microinfarct and comprise the neurites of the plaque. Neurons directly within the microhemorrhage would die acutely. Neuronal processes caught in the microinfarct and penumbral domain would also be at risk. Damage to neuronal terminals within the microhemorrhage would not remain local but would propagate anterogradely and retrogradely from the local site of injury, possibly continuing trans-synaptically (Liu et al., 2012). In this scenario, perivascular swollen neurites of the NP may be the origin of Hp-tau–positive neurites throughout the neuropil, eventually leading to tangles within neurons in the periplaque infarct region and in projecting brain regions, so that both local and distal neurons would be affected.

Microvascular degeneration in widespread cortical and subcortical areas followed by retrograde degeneration from the point of insult would produce a complex pattern of tangles across local and projecting brain regions. Neuronal populations with terminals closely apposed to cortical microvessels, such as the cholinergic basal forebrain nucleus basalis (Sato et al., 2001), known to degenerate early in AD (Cullen et al., 1997), may account for the early susceptibility of these neuronal populations in the neurodegenerative pattern in AD.

In support of this concept is the finding that basal forebrain tangles appear retrograde to isolated large vessel infarcts (Kato et al., 1988). More generally, this hypothesis can also account for the frequent observation of tangles in stroke (de la Torre, 2006). There is an important and relatively untapped potential in reconciliation of the definitions and sequela of macrobleeds and microbleeds (Chiang et al., 2015; Greenberg et al., 2009) alongside the pericapillary microscopic bleeds shown in the current report. Neurons with dense and widespread cortical connectivity, such as in entorhinal/hippocampal area, would be most vulnerable to widespread capillary breakdown across the cerebral cortex increased probability of their projecting axons passing near a microhemorrhage in the cortex. This mechanism is testable in animal models. This model lends itself to theoretical models of microhemorrhage accumulation alongside anatomical maps of neuronal projections and tangle distribution.

4.7. Conclusion

The microvascular hypothesis for neuritic plaque initiation and resolution has potential to unify several key observations in AD lesion initiation and chronicity. Reduced microvascular blood flow potentially exacerbates neuritic degeneration, amyloid angiopathy, and AD pathology and could be tested in transgenic Aβ and tau animal models (Okamoto et al., 2012; Saito and Ihara, 2016). Neuritic pathology has been linked to microvascular damage in AD (Delacourte et al., 1987), head injury, and animal models (Li et al., 2015; McKee et al., 2009; Perez et al., 2013), with increased Hp-tau in cerebrospinal fluid in cases with cortical microbleeds

(Chiang et al., 2015). AD-type pathology frequently accompanies cerebrovascular pathology (Blair et al. 2015; Li et al., 2015; McKee et al., 2009; Perez et al., 2013). Notably, in a young case with DS/AD, as well as in early-onset AD cases, the perivascular focus of NPs is consistent, suggesting the proximity of NP neurites to compromised microvessels is a general feature of the NP lesion and not solely due to aging. However, aging of the microvasculature and accumulated cerebrovascular pathology with age remains a likely contributor to microvascular infarcts.

A growing body of evidence supports the notion that the pathophysiology of AD fundamentally involves cerebrovascular pathology. Several epidemiologic analyses from large population studies consistently find that cardiovascular risk factors are also strong risk factors for AD (Breteler, 2000; Calik et al., 2014; Carnevale et al., 2016; de Bruijn and Ikram, 2014; Ferreira et al., 2014; Launer, 2002, 2009; Love and Miners, 2016; Ruitenberg et al., 2005; Saito and Ihara, 2016; Skoog and Gustafson, 2003). The microvasculature is vulnerable in AD, with reports of microvessel tortuosity and density changes (Buee et al., 1994), endothelial degeneration (Cullen et al., 2005; Hunter et al., 2012; Kalaria and Hedera, 1995), and microhemorrhages (Cullen et al., 2005; Okamoto et al., 2009). Additional insights into precipitating factors in microvascular degeneration can be predicted to emerge from continued large population studies. From an individual and public health perspective, many cardiovascular risk factors for AD are modifiable and can tap into development of cerebrovascular therapy targets (Hawkes et al., 2011; Kuller, 2006; Love and Miners, 2016; Saito and Ihara, 2016). There are near-term advantages for adopting a perspective on AD pathogenesis that includes microvascular pathology, including reinforcement of public health messages aimed at vascular health and for in vivo tracking of microhemorrhages in the progression of AD.

Disclosure

None of the funding sources had any involvement in the collection, analysis, or interpretation of data, writing of the report, or in the decision to submit this article for publication.

Acknowledgements

The authors acknowledge the access to invaluable tissue resource supported by the National Health and Medical Research Council Network for Brain Research into Mental Health. Brain tissue was obtained from Victorian Brain Bank Network, The University of Melbourne, and the Mental Health Research Institute of Victoria, Australia. Thank you to Professor Bogdan Dreher for support and guidance through this project.

This work was supported by the Rebecca L. Cooper Foundation, the J. J. Mason and H. S. Williams Memorial Foundation, and the NWG Macintosh Memorial Fund, Discipline of Anatomy & Histology, University of Sydney.

This study has been approved by the Human Research and Ethics Committee of the University of Sydney, approval number 2013/070.

All authors have reviewed the contents of the manuscript being submitted and approve of the contents and validate the accuracy of the data.

Authors' contributions: GKH, GP, and POB are equal coauthors. GKH, GP, POB, TJ, and MV contributed to tissue labeling, microscopy, and image analysis and data analysis. CG contributed to data analysis and manuscript production. KMC was responsible for study design, tissue collection, and processing, image analysis, and manuscript production.

Appendix A. Supplementary data

Supplementary data to this article can be found online at https://doi.org/10.1016/j.neurobiolaging.2019.06.009.

References

Arriagada, P.V., Growden, J.H., Hedley-Whyte, T., Hyman, B.T., 1992. Neurofibrillary tangles but not senile plaques parallel duration and severity of Alzheimer's disease. Neurology 42, 631–639.
Attwell, D., Buchan, A.M., Charpak, S., Lauritzen, M., Macvicar, B.A., Newman, E.A., 2010. Glial and neuronal control of brain blood flow. Nature 468, 232–243.
Atwood, C.S., Bowen, R.L., Smith, M.A., Perry, G., 2003. Cerebrovascular requirement for sealant, anti-coagulant and remodeling molecules that allow for the maintenance of vascular integrity and blood supply. Brain Res. Brain Res. Rev. 43, 164–178.
Bancher, C., Braak, H., Fischer, P., Jellinger, K., 1993. Neuropathological staging of Alzheimer lesions and intellectual status in Alzheimer's and Parkinson's disease patients. Neurosci. Lett. 162, 179–182.
Benarroch, E., 2007. Neurovascular unit dysfunction: a vascular component of Alzheimer disease? Neurology 68, 1730–1732.
Blair, L.J., Frauen, H.D., Zhang, B., Nordhues, B.A., Bijan, S., Lin, Y.-C., Zamudio, F., Hernandez, L.D., Sabbagh, J.J., Selenica, M.-L.B., Dickey, C.A., 2015. Tau depletion prevents progressive blood-brain barrier damage in a mouse model of tauopathy. Acta Neuropathol. Commun. 3, 8.
Braak, H., Braak, E., 1988. Neuropil threads occur in dendrites of tangle-bearing nerve cells. Neuropathol. Appl. Neurobiol. 14, 39–44.
Braak, H., Braak, E., 1991. Neuropathological stageing of Alzheimer-related changes. Acta Neuropathol. 82, 239–259.
Breteler, M.M., Bots, M.L., Ott, A., Hofman, A., 1998. Risk factors for vascular disease and dementia. Haemostasis 28, 167–173.
Breteler, M.M.B., 2000. Vascular risk factors for Alzheimer's disease: an epidemiologic perspective. Neurobiol. Aging 21, 153–160.
Brown, W.R., Moody, D.M., Thore, C.R., Challa, V.R., 2000. Cerebrovascular pathology in Alzheimer's disease and leukoaraiosis. Ann. N. Y. Acad. Sci. 903, 39–45.
Buee, L., Hof, P., Bouras, C., Delacourte, A., Perl, D., Morrison, J., Fillit, H., 1994. Pathological alterations of the cerebral microvasculature in Alzheimer's disease and related dementing disorders. Acta Neuropathol. 87, 469–480.
Burdo, J.R., Connor, J.R., 2003. Brain iron uptake and homeostatic mechanisms: an overview. Biometals 16, 63–75.
Bush, A.I., Tanzi, R.E., 2008. Therapeutics for Alzheimer's disease based on the metal hypothesis. Neurotherapeutics 5, 421–432.
Calik, A.N., Ozcan, K.S., Yuksel, G., Gungor, B., Arugarslan, E., Varlibas, F., Ekmekci, A., Osmonov, D., Tatlisu, M.A., Karaca, M., Bolca, O., Erdinler, I., 2014. Altered diastolic function and aortic stiffness in Alzheimer's disease. Clin. Interv. Aging 9, 1115–1121.
Carnevale, D., Perrotta, M., Lembo, G., Trimarco, B., 2016. Pathophysiological links among hypertension and Alzheimer's disease. High Blood Press. Cardiovasc. Prev. 23, 3–7.
Castellani, R.J., Moreira, P.I., Perry, G., Zhu, X., 2012. The role of iron as a mediator of oxidative stress in Alzheimer disease. Biofactors 38, 133–138.
Challa, V.R., Thore, C.R., Moody, D.M., Brown, W.R., Anstrom, J.A., 2002. A three-dimensional study of brain string vessels using celloidin sections stained with anti-collagen antibodies. J. Neurol. Sci. 203-204, 165–167.
Chen, H., Chopp, M., Schultz, L., Bodzin, G., Garcia, J.H., 1993. Sequential neuronal and astrocytic changes after transient middle cerebral artery occlusion in the rat. J. Neurol. Sci. 118, 109–116.
Chen, M., Inestrosa, N.C., Ross, G.S., Fernandez, H.L., 1995. Platelets are the primary source of amyloid beta-peptide in human blood. Biochem. Biophys. Res. Commun. 213, 96–103.
Chen, X.H., Siman, R., Iwata, A., Meaney, D.F., Trojanowski, J.Q., Smith, D.H., 2004. Long-term accumulation of amyloid-beta, beta-secretase, presenilin-1, and caspase-3 in damaged axons following brain trauma. Am. J. Pathol. 165, 357–371.
Chiang, G.C., Cruz Hernandez, J.C., Kantarci, K., Jack, C.R., Weiner, M.W., 2015. Cerebral microbleeds, CSF p-tau, and cognitive decline: significance of anatomic distribution. AJNR Am. J. Neuroradiol. 36, 1635–1641.
Connor, J.R., Menzies, S.L., St Martin, S.M., Mufson, E.J., 1992. A histochemical study of iron, transferrin, and ferritin in Alzheimer's diseased brains. J. Neurosci. Res. 31, 75–83.
Cortes-Canteli, M., Zamolodchikov, D., Ahn, H.J., Strickland, S., Norris, E.H., 2012. Fibrinogen and altered hemostasis in Alzheimer's disease. J. Alzheimers Dis. 32, 599–608.
Cristovao, J.S., Santos, R., Gomes, C.M., 2016. Metals and neuronal metal binding proteins implicated in Alzheimer's disease. Oxid. Med. Cell Longev. 2016, 9812178.
Cullen, K.M., 1997. Perivascular astrocytes within Alzheimer's disease plaques. Neuroreport 8, 1961–1966.
Cullen, K.M., Halliday, G.M., Double, K.L., Brooks, W.S., Creasey, H., Broe, G.A., 1997. Cell loss in the nucleus basalis is related to regional cortical atrophy in Alzheimer's disease. Neuroscience 78, 641–652.
Cullen, K.M., Kocsi, Z., Stone, J., 2005. Pericapillary haem-rich deposits: evidence for microhaemorrhages in aging human cerebral cortex. J. Cereb. Blood Flow Metab. 25, 1656–1667.

Cullen, K.M., Kocsi, Z., Stone, J., 2006. Microvascular pathology in the aging human brain: evidence that senile plaques are sites of microhaemorrhages. Neurobiol. Aging 27, 1786–1796.
de Bruijn, R.F., Ikram, M.A., 2014. Cardiovascular risk factors and future risk of Alzheimer's disease. BMC Med. 12, 130.
De Jong, G.I., Farkas, E., Stienstra, C.M., Plass, J.R., Keijser, J.N., de la Torre, J.C., Luiten, P.G., 1999. Cerebral hypoperfusion yields capillary damage in the hippocampal CA1 area that correlates with spatial memory impairment. Neuroscience 91, 203–210.
De La Torre, J.C., 2000. Impaired cerebromicrovascular perfusion: summary of evidence in support of its causality in Alzheimer's disease. Ann. N. Y. Acad. Sci. 924, 136–152.
de la Torre, J.C., 2006. How do heart disease and stroke become risk factors for Alzheimer's disease? Neurol. Res. 28, 637–644.
Delacourte, A., Defossez, A., Persuy, P., Peers, M.C., 1987. Observation of morphological relationships between angiopathic blood vessels and degenerative neurites in Alzheimer's disease. Virchows Arch. A. Pathol. Anat. Histopathol. 411, 199–204.
Farkas, E., De Vos, R.A.I., Steur, E.N.H., Luiten, P.G.M., 2000. Are Alzheimer's disease, hypertension and cerebrocapillary damage related? Neurobiol. Aging 21, 235–243.
Ferreira, L.K., Tamashiro-Duran, J.H., Squarzoni, P., Duran, F.L., Alves, T.C., Buchpiguel, C.A., Busatto, G.F., 2014. The link between cardiovascular risk, Alzheimer's disease, and mild cognitive impairment: support from recent functional neuroimaging studies. Braz. J. Psychiatry 36, 344–357.
Furcila, D., DeFelipe, J., Alonso-Nanclares, L., 2018. A study of amyloid-beta and phosphotau in plaques and neurons in the Hippocampus of Alzheimer's disease patients. J. Alzheimers Dis. 64, 417–435.
Garton, T., Keep, R.F., Hua, Y., Xi, G., 2016. Brain iron overload following intracranial haemorrhage. Stroke Vasc. Neurol. 1, 172–184.
Grammas, P., Yamada, M., Zlokovic, B., 2002. The cerebromicrovasculature: a key player in the pathogenesis of Alzheimer's disease. J. Alzheimers Dis. 4, 217–223.
Greenberg, S.M., Nandigam, R.N., Delgado, P., Betensky, R.A., Rosand, J., Viswanathan, A., Frosch, M.P., Smith, E.E., 2009. Microbleeds versus macrobleeds: evidence for distinct entities. Stroke 40, 2382–2386.
Guillemin, G.J., Brew, B.J., Noonan, C.E., Takikawa, O., Cullen, K.M., 2005. Indoleamine 2,3 dioxygenase and quinolinic acid Immunoreactivity in Alzheimer's disease hippocampus. Neuropathol. Appl. Neurobiol. 31, 395–404.
Hamel, E., 2006. Perivascular nerves and the regulation of cerebrovascular tone. J. Appl. Physiol. 100, 1059–1064.
Hawkes, C.A., Gatherer, M., Sharp, M.M., Dorr, A., Yuen, H.M., Kalaria, R., Weller, R.O., Carare, R.O., 2013. Regional differences in the morphological and functional effects of aging on cerebral basement membranes and perivascular drainage of amyloid-beta from the mouse brain. Aging Cell 12, 224–236.
Hawkes, C.A., Hartig, W., Kacza, J., Schliebs, R., Weller, R.O., Nicoll, J.A., Carare, R.O., 2011. Perivascular drainage of solutes is impaired in the ageing mouse brain and in the presence of cerebral amyloid angiopathy. Acta Neuropathol. 121, 431–443.
Hunter, J.M., Kwan, J., Malek-Ahmadi, M., Maarouf, C.L., Kokjohn, T.A., Belden, C., Sabbagh, M.N., Beach, T.G., Roher, A.E., 2012. Morphological and pathological evolution of the brain microcirculation in aging and Alzheimer's disease. PLoS One 7, e36893.
Jellinger, K.A., 2002. Alzheimer disease and cerebrovascular pathology: an update. J. Neural. Transm. 109, 813–836.
Kalaria, R.N., 2002. Small vessel disease and Alzheimer's dementia: pathological considerations. Cerebrovasc. Dis. 13 (Suppl.2), 48–52.
Kalaria, R.N., Hedera, P., 1995. Differential degeneration of the cerebral microvasculature in Alzheimer's disease. Neuroreport 6, 477–480.
Kato, T., Hirano, A., Katagiri, T., Sasaki, H., Yamada, S., 1988. Neurofibrillary tangle formation in the nucleus basalis of Meynert ipsilateral to a massive cerebral infarct. Ann. Neurol. 23, 620–623.
King, C.E., Jacobs, I., Dickson, T.C., Vickers, J.C., 1997. Physical damage to rat cortical axons mimics early Alzheimer's neuronal pathology. Neuroreport 8, 1663–1665.
Koeppen, A.H., 2003. A brief history of brain iron research. J. Neurol. Sci. 207, 95–97.
Koeppen, A.H., Dickson, A.C., McEvoy, J.A., 1995. The cellular reactions to experimental intracerbral haemorrhage. J. Neurol. Sci. 134S, 102–112.
Kuller, L.H., 2006. Dementia epidemiology research: it is time to modify the focus of research. J. Gerontol. A. Biol. Sci. Med. Sci. 61, 1314–1318.
Kumar-Singh, S., Pirici, D., McGowan, E., Serneels, S., Ceuterick, C., Hardy, J., Duff, K., Dickson, D., Van Broeckhoven, C., 2005. Dense-core plaques in Tg2576 and PSAPP mouse models of Alzheimer's disease are centered on vessel walls. Am. J. Pathol. 167, 527–543.
Launer, L.J., 2002. Demonstrating the case that AD is a vascular disease: epidemiologic evidence. Ageing Res. Rev. 1, 61–77.
Launer, L.J.P., 2009. Diabetes: vascular or neurodegenerative: an epidemiologic perspective. Stroke 40, S53–S55.
Lecrux, C., Hamel, E., 2011. The neurovascular unit in brain function and disease. Acta Physiol. 203, 47–59.
Lee, J.-Y., Keep, R.F., He, Y., Sagher, O., Hua, Y., Xi, G., 2010. Hemoglobin and iron handling in brain after subarachnoid hemorrhage and the effect of deferoxamine on early brain injury. J. Cereb. Blood Flow Metab. 30, 1793–1803.
LeVine, S.M., 1997. Iron deposits in multiple sclerosis and Alzheimer's disease brains. Brain Res. 760, 298–303.
Li, J.M., Cai, Y., Liu, F., Yang, L., Hu, X., Patrylo, P.R., Cai, H., Luo, X.G., Xiao, D., Yan, X.X., 2015. Experimental microembolism induces localized neuritic pathology in Guinea pig cerebrum. Oncotarget 6, 10772–10785.
Liu, B., Moloney, A., Meehan, S., Morris, K., Thomas, S.E., Serpell, L.C., Hider, R., Marciniak, S.J., Lomas, D.A., Crowther, D.C., 2011. Iron promotes the toxicity of amyloid beta peptide by impeding its ordered aggregation. J. Biol. Chem. 286, 4248–4256.
Liu, J.-L., Fan, Y.-G., Yang, Z.-S., Wang, Z.-Y., Guo, C., 2018. Iron and Alzheimer's disease: from pathogenesis to therapeutic implications. Front. Neurosci. 12, 632.
Liu, L., Drouet, V., Wu, J.W., Witter, M.P., Small, S.A., Clelland, C., Duff, K., 2012. Trans-Synaptic spread of tau pathology in vivo. PLoS One 7, e31302.
Love, S., Miners, J.S., 2016. Cerebrovascular disease in ageing and Alzheimer's disease. Acta Neuropathol. 131, 645–658.
Macchi, G., Brahe, C., Pomponi, M., 1997. Alois Alzheimer and Gaetano Perusini: should man divide what fate united? Eur. J. Neurol. 4, 210–213.
McKee, A.C., Cantu, R.C., Nowinski, C.J., Hedley-Whyte, E.T., Gavett, B.E., Budson, A.E., Santini, V.E., Lee, H.-S., Kubilus, C.A., Stern, R.A., 2009. Chronic traumatic encephalopathy in athletes: progressive tauopathy after repetitive head injury. J. Neuropathol. Exp. Neurol. 68, 709–735.
Mesulam, M., 2000. A plasticity-based theory of the pathogenesis of Alzheimer's disease. Ann. N. Y. Acad. Sci. 924, 42–52.
Michael, R., Lenferink, A., Vrensen, G.F.J.M., Gelpi, E., Barraquer, R.I., Otto, C., 2017. Hyperspectral Raman imaging of neuritic plaques and neurofibrillary tangles in brain tissue from Alzheimer's disease patients. Sci. Rep. 7, 15603.
Montagne, A., Barnes, S.R., Sweeney, M.D., Halliday, M.R., Sagare, A.P., Zhao, Z., Toga, A.W., Jacobs, R.E., Liu, C.Y., Amezcua, L., Harrington, M.G., Chui, H.C., Law, M., Zlokovic, B.V., 2015. Blood-brain barrier breakdown in the aging human hippocampus. Neuron 85, 296–302.
Moreira, P.I., Siedlak, S.L., Aliev, G., Zhu, X., Cash, A.D., Smith, M.A., Perry, G., 2005. Oxidative stress mechanisms and potential therapeutics in Alzheimer disease. J. Neural. Transm. 112, 921–932.
Morris, J.C., Heyman, A., Mohs, R.C., Hughes, J.P., van Belle, G., Fillenbaum, G., Mellits, E.D., Clark, C., 1994. The consortium to establish a registry for Alzheimer's disease (CERAD). Part I. Clinical and neuropsychological assessment of Alzheimer's disease. Neurology 39, 1159–1165.
Nation, D.A., Sweeney, M.D., Montagne, A., Sagare, A.P., D'Orazio, L.M., Pachicano, M., Sepehrband, F., Nelson, A.R., Buennagel, D.P., Harrington, M.G., Benzinger, T.L.S., Fagan, A.M., Ringman, J.M., Schneider, L.S., Morris, J.C., Chui, H.C., Law, M., Toga, A.W., Zlokovic, B.V., 2019. Blood–brain barrier breakdown is an early biomarker of human cognitive dysfunction. Nat. Med. 25, 270–276.
Nitatori, T., Sato, N., Waguri, S., Karasawa, Y., Araki, H., Shibanai, K., Kominami, E., Uchiyama, Y., 1995. Delayed neuronal death in the CA1 pyramidal cell layer of the gerbil hippocampus following transient ischemia is apoptosis. J. Neurosci. 15, 1001–1011.
Nübling, G., Bader, B., Levin, J., Hildebrandt, J., Kretzschmar, H., Giese, A., 2012. Synergistic influence of phosphorylation and metal ions on tau oligomer formation and coaggregation with α-synuclein at the single molecule level. Mol. Neurodegener. 7, 35.
Okamoto, Y., Ihara, M., Fujita, Y., Ito, H., Takahashi, R., Tomimoto, H., 2009. Cortical microinfarcts in Alzheimer's disease and subcortical vascular dementia. Neuroreport 20, 990–996.
Okamoto, Y., Yamamoto, T., Kalaria, R.N., Senzaki, H., Maki, T., Hase, Y., Kitamura, A., Washida, K., Yamada, M., Ito, H., Tomimoto, H., Takahashi, R., Ihara, M., 2012. Cerebral hypoperfusion accelerates cerebral amyloid angiopathy and promotes cortical microinfarcts. Acta Neuropathol. 123, 381–394.
Osuga, H., Hakim, A., 1994. Relevance of interstitial glutamate to selective vulnerability in focal cerebral ischemia. J. Cereb. Blood Flow Metab. 14, 343–347.
Park, J.S., Bateman, M.C., Goldberg, M.P., 1996. Rapid alterations in dendrite morphology during sublethal hypoxia or glutamate receptor acivation. Neurobiol. Dis. 3, 215–227.
Perez, S.E., Raghanti, M.A., Hof, P.R., Kramer, L., Ikonomovic, M.D., Lacor, P.N., Erwin, J.M., Sherwood, C.C., Mufson, E.J., 2013. Alzheimer's disease pathology in the neocortex and hippocampus of the western lowland gorilla (Gorilla gorilla gorilla). J. Comp. Neurol. 521, 4318–4338.
Pluta, R., 1997. Experimental model of neuropathological changes characteristic for Alzheimer's disease. Folia Neuropathol. 35, 94–98.
R Core Team, 2015. R: A Language and Environment for Statistical Computing. R Foundation for Statistical Computing. Vienna, Austria. https://www.R-project.org. (Accessed 30 January 2017).
Rahman, A., Ting, K., Cullen, K.M., Braidy, N., Brew, B.J., Guillemin, G.J., 2009. The excitotoxin quinolinic acid induces tau phosphorylation in human neurons. PLoS One 4, e6344.
Rao, S.S., Adlard, P.A., 2018. Untangling tau and iron: exploring the interaction between iron and tau in neurodegeneration. Front. Mol. Neurosci. 11, 276.
Raz, L., Bhaskar, K., Weaver, J., Marini, S., Zhang, Q., Thompson, J.F., Espinoza, C., Iqbal, S., Maphis, N.M., Weston, L., Sillerud, L.O., Caprihan, A., Pesko, J.C., Erhardt, E.B., Rosenberg, G.A., 2019. Hypoxia promotes tau hyperphosphorylation with associated neuropathology in vascular dysfunction. Neurobiol. Dis. 126, 124–136.
Roher, A.E., Esh, C., Kokjohn, T.A., Kalback, W., Luehrs, D.C., Seward, J.D., Sue, L.I., Beach, T.G., 2003. Circle of Willis Atherosclerosis is a risk factor for sporadic Alzheimer's disease. Arterioscler. Thromb. Vasc. Biol. 23, 2055–2062.
Rovelet-Lecrux, A., 2006. APP locus duplication causes autosomal dominant early-onset Alzheimer disease with cerebral amyloid angiopathy. Nat. Genet. 38, 24–26.
Ruitenberg, A., den Heijer, T., Bakker, S.L., van Swieten, J.C., Koudstaal, P.J., Hofman, A., Breteler, M.M., 2005. Cerebral hypoperfusion and clinical onset of dementia: the Rotterdam Study. Ann. Neurol. 57, 789–794.

Saito, S., Ihara, M., 2016. Interaction between cerebrovascular disease and Alzheimer pathology. Curr. Opin. Psychiatry 29, 168–173.
Sato, A., Sato, Y., Uchida, S., 2001. Regulation of regional cerebral blood flow by cholinergic fibers originating in the basal forebrain. Int. J. Dev. Neurosci. 19, 327–337.
Scheibel, A.B., Duong, T.H., Jacobs, R., 1989. Alzheimer's disease as a capillary dementia. Ann. Med. 21, 103–107.
Schindelin, J., Arganda-Carreras, I., Frise, E., Kaynig, V., Longair, M., Pietzsch, T., Preibisch, S., Rueden, C., Saalfeld, S., Schmid, B., Tinevez, J.Y., White, D.J., Hartenstein, V., Eliceiri, K., Tomancak, P., Cardona, A., 2012. 2012. Fiji: an open-source platform for biological-image analysis. Nat. Methods 9, 676–682.
Schönheit, B., Zarski, R., Ohm, T.G., 2004. Spatial and temporal relationships between plaques and tangles in Alzheimer-pathology. Neurobiol. Aging 25, 697–711.
Skoog, I., Gustafson, D., 2003. Hypertension, hypertension-clustering factors and Alzheimer's disease. Neurol. Res. 25, 675–680.
Smith, M.A., Harris, P.L.R., Sayre, L.M., Perry, G., 1997. Iron accumulation in Alzheimer disease is a source of redox-generated free radicals. Proc. Natl. Acad. Sci. U. S. A. 94, 9866.
Stachowski, E.K., Schwarcz, R., 2012. Regulation of quinolinic acid neosynthesis in mouse, rat and human brain by iron and iron chelators in vitro. J. Neural. Transm. 119, 123–131.
Suo, Z., Wu, M., Citron, B.A., Palazzo, R.E., Festoff, B.W., 2003. Rapid tau aggregation and delayed hippocampal neuronal death induced by persistent thrombin signaling. J. Biol. Chem. 278, 37681–37689.
Thomas, T., Miners, S., Love, S., 2015. Post-mortem assessment of hypoperfusion of cerebral cortex in Alzheimer's disease and vascular dementia. Brain 138, 1059–1069.
Tiraboschi, P., Hansen, L.A., Thal, L.J., Corey-Bloom, J., 2004. The importance of neuritic plaques and tangles to the development and evolution of AD. Neurology 62, 1984–1989.
Wagner, K., Sharp, F., Ardizzone, T., Lu, A., Clark, J., 2003. Heme and iron metabolism: role in cerebral hemorrhage. J. Cereb. Blood Flow Metab. 23, 629–652.
Wu, C.W., Liao, P.C., Yu, L., Wang, S.T., Chen, S.T., Wu, C.M., Kuo, Y.M., 2004. Hemoglobin promotes Abeta oligomer formation and localizes in neurons and amyloid deposits. Neurobiol. Dis. 17, 367–377.
Wu, J., Hua, Y., Keep, R.F., Schallert, T., Hoff, J.T., Xi, G., 2002. Oxidative brain injury from extravasated erythrocytes after intracerebral hemorrhage. Brain Res. 953, 45–52.
Yilmazer-Hanke, D.M., Hanke, J., 1999. Progression of Alzheimer-related neuritic plaque pathology in the entorhinal region, perirhinal cortex and hippocampal formation. Dement. Geriatr. Cogn. Disord. 10, 70–76.
Yip, S., Sastry, B., 2000. Effects of hemoglobin and its breakdown products on synaptic transmission in rat hippocampal CA1 neurons. Brain Res. 864, 1–12.
Zlokovic, B.V., 2005. Neurovascular mechanisms of Alzheimer's neurodegeneration. Trends Neurosci. 28, 202–208.